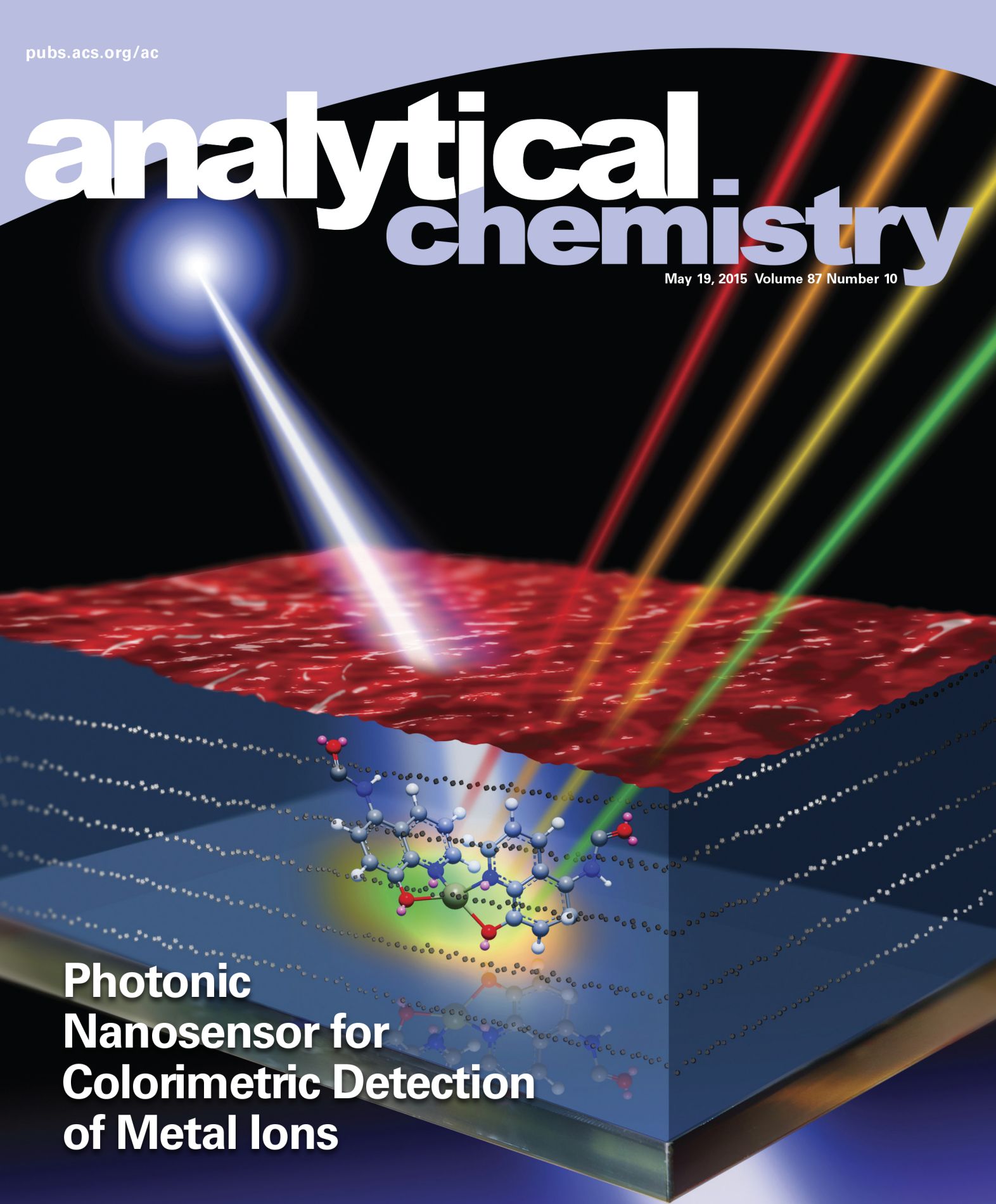


analytical-chemistry

May 19, 2015 Volume 87 Number 10



Photonic Nanosensor for Colorimetric Detection of Metal Ions

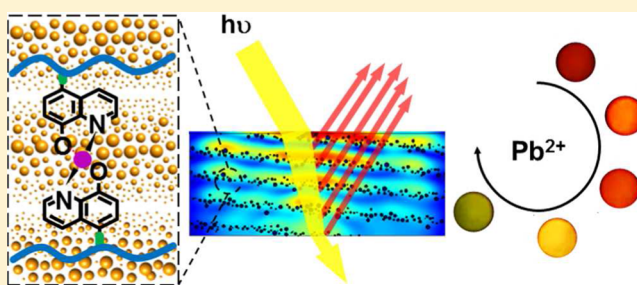


Photonic Nanosensor for Colorimetric Detection of Metal Ions

Ali K. Yetisen,^{*,†} Yunuen Montelongo,[‡] Malik M. Qasim,[‡] Haider Butt,[§] Timothy D. Wilkinson,[‡] Michael J. Monteiro,^{||} and Seok Hyun Yun[†][†]Harvard Medical School and Wellman Center for Photomedicine, Massachusetts General Hospital, 50 Blossom Street, Boston, Massachusetts 02114, United States[‡]Centre of Molecular Materials for Photonics and Electronics, Department of Engineering, University of Cambridge, 9 JJ Thomson Avenue, Cambridge CB3 0FA, United Kingdom[§]School of Mechanical Engineering, University of Birmingham, Edgbaston, Birmingham B15 2TT, United Kingdom^{||}Australian Institute for Bioengineering and Nanotechnology, University of Queensland, Brisbane, Queensland 4072, Australia

Supporting Information

ABSTRACT: The real-time sensing of metal ions at point of care requires integrated sensors with low energy and sample consumption, reversibility, and rapid recovery. Here, we report a photonic nanosensor that reversibly and quantitatively reports on variation in the concentrations of Pb^{2+} and Cu^{2+} ions in aqueous solutions ($<500 \mu\text{L}$) in the visible region of the spectrum ($\lambda_{\text{max}} \approx 400\text{--}700 \text{ nm}$). A single 6 ns laser pulse ($\lambda = 532 \text{ nm}$) was used to pattern an $\sim 10 \mu\text{m}$ thick photosensitive recording medium. This formed periodic AgBr nanocrystal ($\phi \sim 5\text{--}20 \text{ nm}$) concentrated regions, which produced Bragg diffraction upon illumination with a white light source. The sensor functionalized with 8-hydroxyquinoline allowed sensing through inducing Donnan osmotic pressure and tuning its lattice spacing. The sensor quantitatively measured Pb^{2+} and Cu^{2+} ion concentrations within the dynamic range of 0.1–10.0 mM with limits of detection of 11.4 and 18.6 μM in under 10 min. The sensor could be reset in 3 min and was reused at least 100 times without compromising its accuracy. The plasmonic nanosensor represents a simple and label-free analytical platform with potential scalability for applications in medical diagnostics and environmental monitoring.



Metal cation sensors have applications ranging from in vitro diagnostics to assessing the quality of water and intracellular sensing.^{1–5} Advanced techniques for quantifying concentrations of metal cations are based on high-resolution inductively coupled plasma mass spectrometry, atomic absorption, or emission spectroscopy.^{6–8} However, these techniques are high-cost, require significant instrumentation, and are nonportable. Other methods involve quantifying concentration of metal cations using fluorescence.^{9,10} Such techniques do not require high-temperature atomization sources but require sample preparation involving organic solvents to allow the cations to bind to selective agents. Practical solutions include ion-selective electrodes (ISEs) that can provide high selectivities and sensitivities for the detection of metal ions such as Na^+ , K^+ , and Cd^{2+} , while being amenable to miniaturization in battery-operated devices. The need for improving the performance and user interface has motivated the investigation of numerous other approaches such as fluorescent chemosensors,^{11–22} DNA-based detection,^{23–31} silica nanotube-based sensors,³² quantum-dot-labeled DNAzymes,³³ polydiacetylene–liposome microarrays,³⁴ catalytic nanomotors,³⁵ click chemistry-based detection,³⁶ and graphene-based sensors.^{37–39} However, optical sensors have emerged as the platform of choice for the detection and

discrimination of metal ions as they (i) enable sterile sensing without sample contamination, (ii) can be miniaturized and multiplexed within lab-on-chip devices, (iii) offer readouts in the visible region, and (iv) are not affected by electromagnetic fields during sampling and testing.⁴⁰ The notable optical sensors for metal ion detection are colorimetric, label/equipment-free, lightweight, and reusable or disposable.^{41–44} These include synthetic receptor or biomodified metal nanoparticles (NPs),⁴⁵ plasmonic nanocavities,^{46,47} phage-bundle nanostructures,⁴⁸ and quantum dots.⁴⁹ Polymerized crystalline colloidal arrays (CCAs) have emerged as a sensitive optical sensing platform.⁵⁰ They are fabricated from monodisperse and highly charged nanospheres that assemble into a close-packed, well-ordered crystalline array due to long-range electrostatic repulsion at low ionic strength.⁵¹ By fixing this crystalline structure in a hydrogel matrix, the CCA could then be used as an optical sensor, which Bragg diffracts at different wavelengths depending on the nanosphere spacing. The main problems with this method are 2-fold: (i) for the CCA to form, ion depletion from the solution requires lengthy dialysis (>1

Received: November 14, 2014

Accepted: February 12, 2015

Published: February 24, 2015

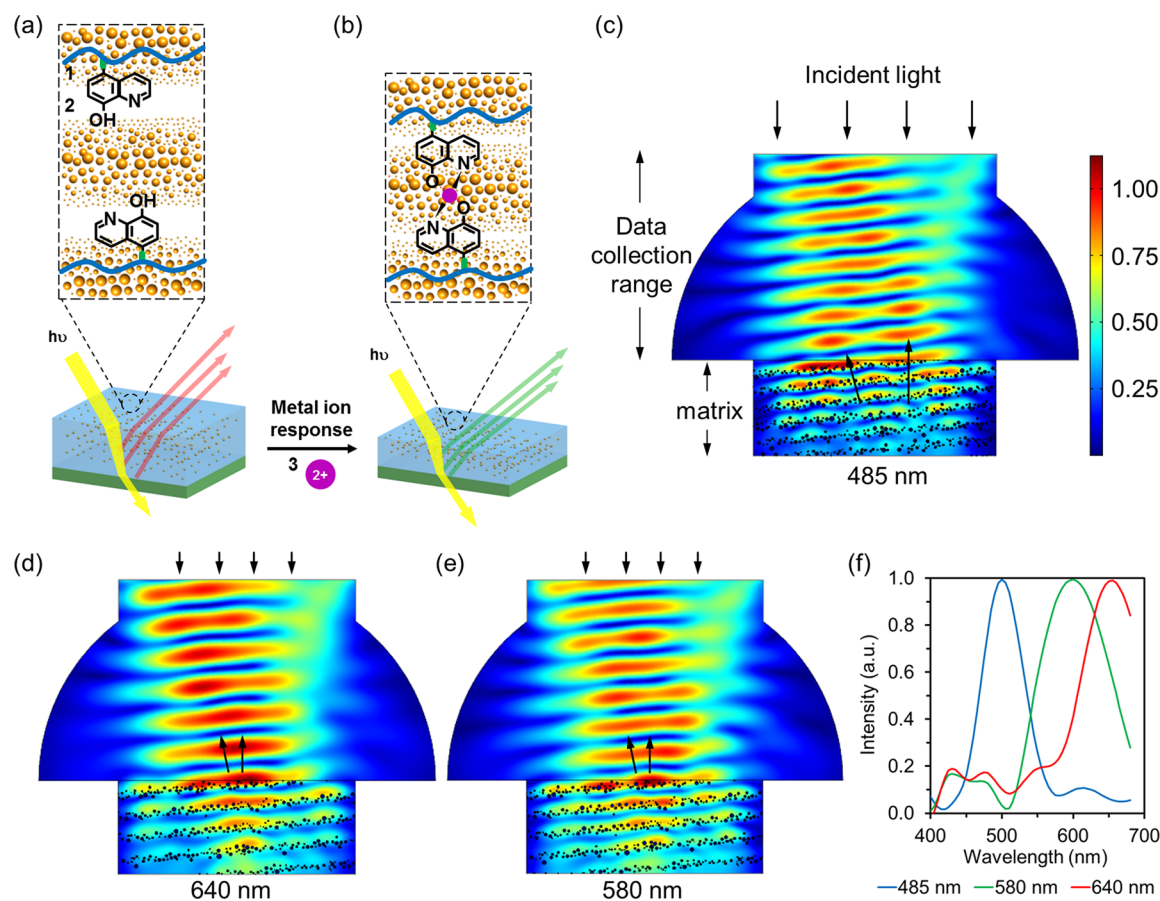


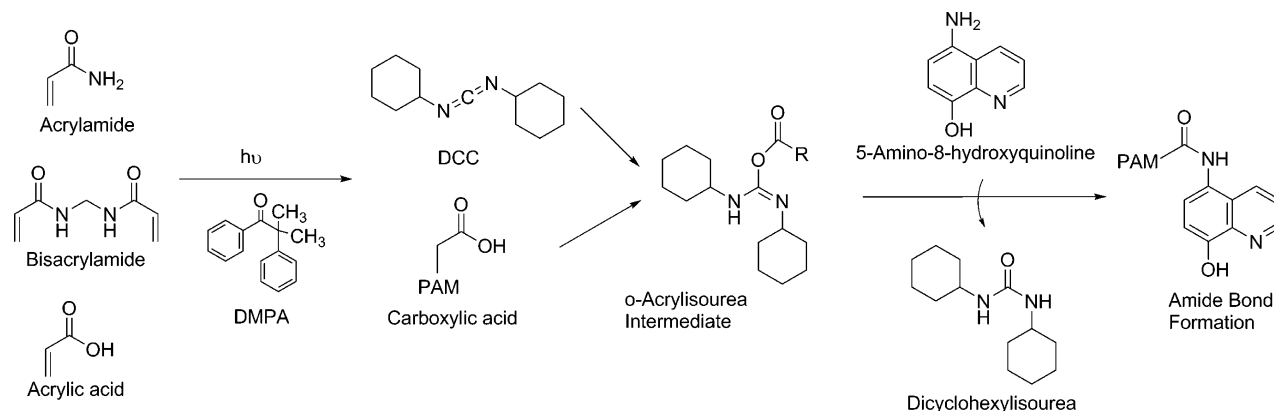
Figure 1. Principle of operation and computational modeling of the NC Bragg grating structure. (a) The structure consists of a PAM matrix 1 that has periodically organized AgBr NCs to diffract narrow-band light. The matrix is functionalized with 8HQ 2 that binds with a divalent metal ion 3, which actuates shrinking in aqueous solutions. (b) Reducing the lattice spacing of the AgBr NCs shifts the Bragg peak to shorter wavelengths. Finite element simulations of (c) 485, (d) 640, and (e) 580 nm waves being diffracted by a slanted grating consisting of AgBr NC stacks in the matrix. The light intensity increases from blue to red. (f) Diffraction spectra of the Bragg grating.

week), and (ii) the cross-linking must not disrupt the array. The latter restricts the inclusion of many functional groups during monomer polymerization. Therefore, functionalization must be performed post hydrogel preparation, resulting in nonuniform distributions of functional moieties throughout the hydrogel matrix.

Here, we create a photonic nanosensor consisting of nanocrystals (NCs) produced in situ within an ionically charged and functional hydrogel using laser writing. This sensor provides a quantitative visual readout of the concentration of divalent metal ions in an aqueous medium and represents an advance on previous detection methods due to its ease of preparation and reusability. Semiquantitative readouts were obtained by visual inspection based on the monochromatic response, and fully quantitative narrow-band readouts were attained through spectrophotometry. The sensor allowed sensing Pb^{2+} and Cu^{2+} ions using a sample volume ($<500 \mu\text{L}$). We demonstrate that the sensor is reusable within 3 min showing reproducibility without hysteresis.

The principle of operation of our sensor is based on the dynamic volume modulation of a poly(acrylamide-*co*-carboxylic acid) (PAM) matrix, which incorporates a AgBr nanocrystal Bragg grating. The AgBr NCs are organized as a multilayer grating in the PAM matrix, which serves as a tunable wavelength filter. Upon illumination with a white light source, the sensor diffracts narrow-band light in the visible region of

the spectrum (Figure 1a). We hypothesized that incorporation of pendant 8-hydroxyquinoline (8HQ) moieties into the matrix and subsequent chelation of divalent metal ions could shift the Bragg peak to shorter wavelengths due to a decrease in the Donnan osmotic pressure (Figure 1b). Computation of the interaction between the photonic structure and the electromagnetic field using finite-difference time domain algorithms provided a theoretical model of the optical properties for the device. Finite element simulations were performed for the diffraction of a light wave at 485 nm propagating through a PAM matrix with 5° slanted and stacked nanostructures (Figure 1c). The AgBr NCs were distributed within the matrix consisting of a multilayer grating confined within a $2.5 \times 1.0 \mu\text{m}^2$ area. Upon illumination with normal incidence, the light was partially reflected, transmitted, and diffracted at $\sim 10^\circ$ from the normal. When the lattice constant matched the effective incident wavelength (λ_{peak}/n), a maximum diffraction efficiency was observed. The wavelengths not satisfying this condition were transmitted and reflected normally without diffraction. Parts d and e of Figure 1 show that, as the lattice spacing decreases from 214 to 194 nm, the Bragg peak shifts from 640 to 580 nm. Figure 1f shows the simulated spectra of the AgBr NC grating and its selective wavelength diffraction.

Scheme 1. Functionalization of PAM with 8HQ^a

^aFree radical polymerization of acrylamide, acrylic acid, and *N,N'*-methylenebis(acrylamide) with a 66:32:3 mol % ratio in the presence of 2-dimethoxy-2-phenylacetophenone (DMPA) and functionalization of the PAM matrix with 8HQ through DCC-initiated condensation reaction.

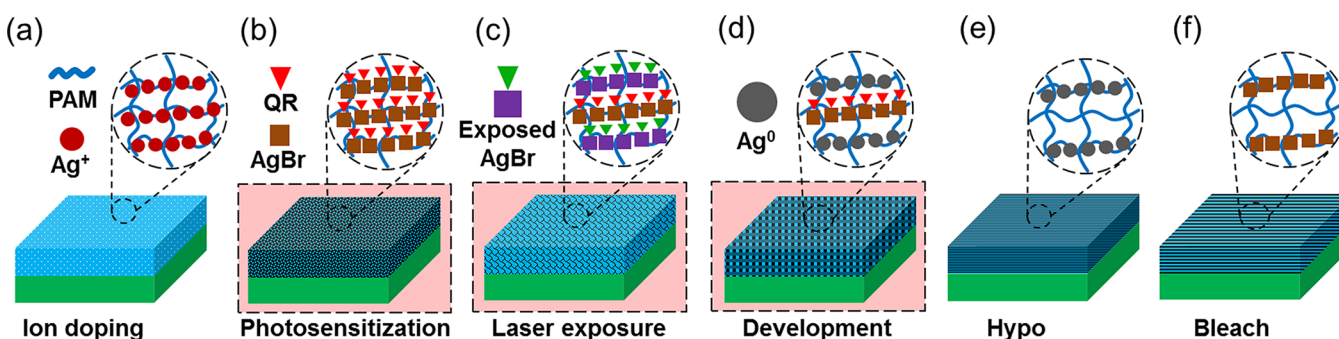


Figure 2. Fabrication of the photonic metal ion sensor through silver halide chemistry. (a) Diffusion of Ag^+ ions into the PAM matrix. (b) Formation of AgBr NCs bound to QR photosensitizing dye in the PAM matrix. (c) Exposure of the system tilted at 5° from the surface of a mirror, using a single pulse of a laser light (532 nm, 6 ns). (d) Development of exposed AgBr NC latent image sites to Ag^0 NPs. (e) Removal of undeveloped AgBr NCs from the PAM matrix using a $\text{Na}_2\text{S}_2\text{O}_3$ solution. (f) Bleaching AgBr NCs with a CuSO_4 and KBr solution in order to convert the Ag^0 NPs to AgBr NCs. Parts b–d were carried out under a red safelight.

EXPERIMENTAL SECTION

Materials. 3-(Trimethoxysilyl)propyl methacrylate (silane), acrylamide (AM) (98%), *N,N'*-methylenebis(acrylamide) (MBAM; 99%), 2-dimethoxy-2-phenylacetophenone (DMPA) (99.0%), acrylic acid (AA) (99%), 5-amino-8-hydroxyquinoline (5A-8HQ) dihydrochloride (95%), *N,N'*-dicyclohexylcarbodiimide (DCC; 99%), triethanolamine (99.0%), lithium chloride (99.0%), lithium bromide (99%), sodium chloride (99.5%), (+)-sodium L-ascorbate (99.0%), sodium carbonate (99.9%), sodium hydroxide (98.0%), sodium thiosulfate (98.0%), L-ascorbic acid (99.0%), potassium chloride (99.0%), potassium bromide (99%), rubidium chloride (99.0%), cesium chloride (99.9%), magnesium chloride hexahydrate (99.0%), calcium chloride (93.0%), barium chloride dehydrate (99%), manganese(II) chloride (99%), iron(II) chloride (98.0%), iron(III) chloride (99.9%), cobalt(II) chloride (97%), nickel(II) chloride (98%), copper(II) chloride (99.0%), copper(II) sulfate (99%), zinc chloride (98%), lead(II) chloride (98%), sodium acetate trihydrate (99.0%), silver nitrate (AgNO_3) (99.0%), 2-(4-dimethylaminostyryl)-1-ethylquinolinium iodide (Quinaldine red photosensitizing dye, 95%), 4-(methylamino)phenol hemisulfate salt (metol, 99%), ethylenediaminetetraacetic acid tetrasodium salt hydrate (Na_4EDTA ; 99.0%), ethylenediaminetetraacetic acid iron(III) sodium salt (Fe(III)-NaEDTA), and qualitative filter paper (Whatman, grade 6, circles, $d = 90$ mm) were purchased from Sigma-Aldrich, U.K.

Ethanol, methanol, acetone, acetic acid (glacial), dimethyl sulfoxide (DMSO), dimethylformamide solution (37%), and glass microscope slides (ground, $t = 1.2$ mm) were purchased from Fisher Scientific. All chemicals were of analytical grade and used without further purification. Ultrapure water (18 $\text{M}\Omega$ cm) (Milli-Q Advantage A10, Millipore) was used for all experiments.

Instruments. Single-side aluminized polyester film was purchased from HiFi Industrial Film Ltd. (Stevenage, U.K.). Stratalinker 2400 UV cross-linker (~ 350 nm, 4000 $\mu\text{watts}/\text{cm}^2$) was purchased from RS Components (Corby, U.K.). Neodymium yttrium aluminum garnet pulsed laser (high-power compact Q-switched Nd:YAG oscillator with super-Gaussian resonator, 700 mJ at 1064 nm, 10 Hz, with a second-harmonic generator, 350 mJ at 532 nm 10 Hz, 6 ns, thermally stabilized with wavelength separation) was purchased from Lambda Photometrics (U.K.). An AveSpec 2028 spectrophotometer, a 2048-pixel InstaSpec IV CCD detector, and bifurcated cable (FC UV 600-2, 600 μm fiber, 2 m length, SMA terminations) were purchased from Avantes (Apeldoorn, Netherlands). Panasonic Lumix DMC-FZ20 camera was used for imaging. AvaSoft (v7.5, Avantes) and SciDAVis (1.D005) were used for data collection and analysis. MATLAB (R2014a, MathWorks) and COMSOL Multiphysics (v4.4) were used for diffraction simulations. pH meter (FE20 FiveEasy, Mettler Toledo) was used for buffer preparation.

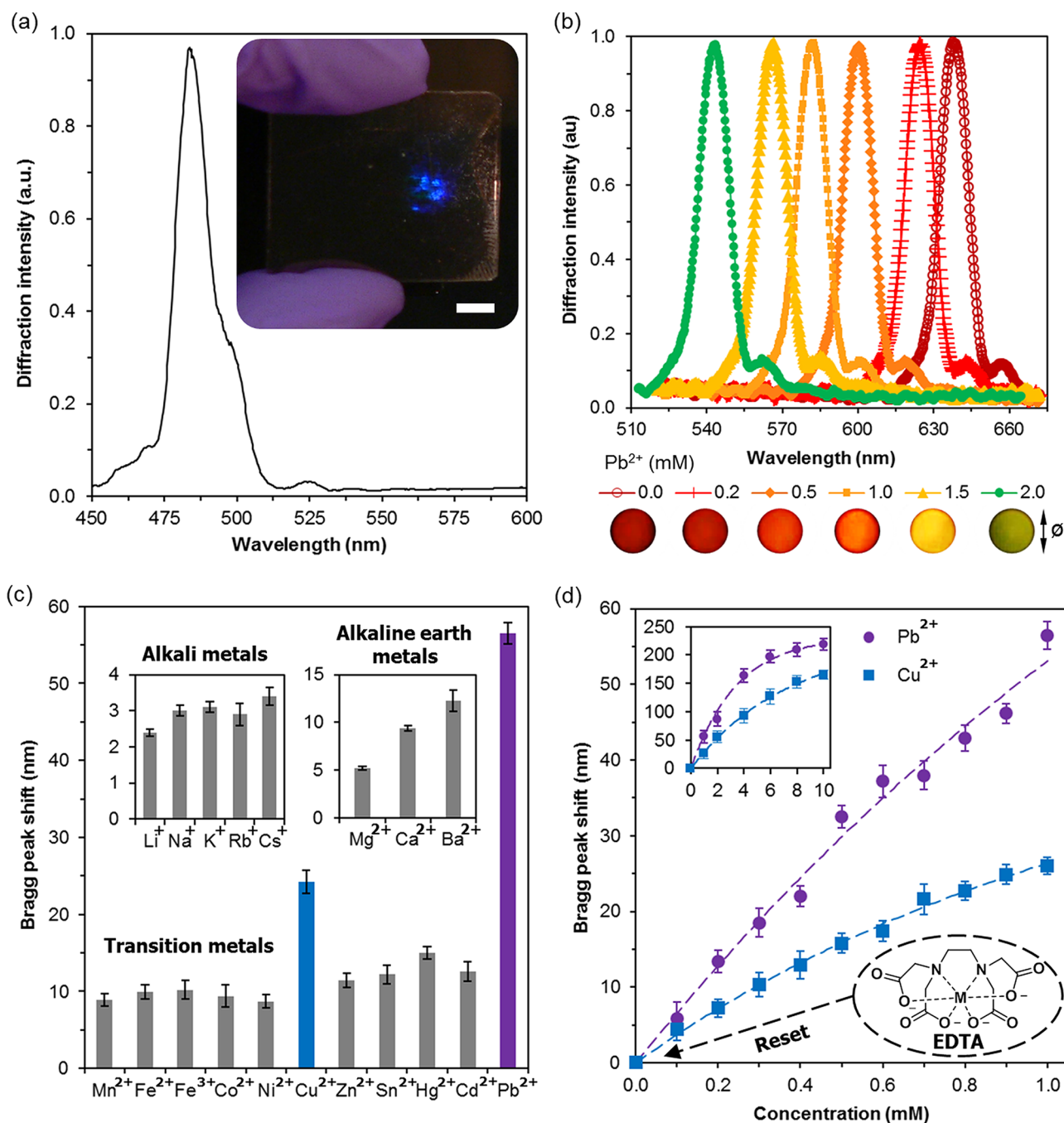


Figure 3. Optical readouts of the photonic metal cation sensor. (a) The diffraction spectrum of the sensor at ambient humidity (60% RH). The inset shows the diffracted narrow-band light at 485 nm when the sensor is illuminated with a white light source. Scale bar = 5 mm. (b) A typical sensor response to an increase in the concentration of Pb^{2+} ions (2.0 mM) in acetate buffers (pH 4.20, 200 mM) at 24 °C. The inset shows the colorimetric response of the sensor as a function of Pb^{2+} ion concentration. $\phi = 3$ mm. (c) Readouts of the sensor to variation in metal ion concentrations (1.0 mM) in acetate buffers (pH 4.2, 200 mM) at 24 °C over 10 min. The sensor displays higher blue Bragg shifts for Pb^{2+} and Cu^{2+} ions than other divalent cations. (d) Sensor readouts for Pb^{2+} and Cu^{2+} ions at 1.0 and 10.0 mM (inset). The dashed lines represent the fitting according to the exponential decay eq 2. Standard error bars represent three independent trials. The initial Bragg peak (λ_{peak}) is 637.0 ± 0.8 nm.

Synthesis of the Photonic Nanosensor. The sensor was fabricated from hydrogel copolymerized with acrylic acid that was layered on a silanized glass slide (Scheme 1). The monomer mixture consisted of AM, MBAM, and AA (Supporting Information Table S-1). The Bragg grating was incorporated into the PAM matrix using silver halide chemistry, which allowed the formation of fine AgBr NCs.⁵² The matrix was impregnated with Ag^+ ions (Figure 2a), followed by its photosensitization by the formation of AgBr NCs in the

presence of dye Quinaldine red (QR, $\lambda_{\text{peak}} = 528$ nm) (Figure 2b). A 6 ns laser operating at 532 nm in Denisyuk reflection mode to produce standing waves photochemically patterned the PAM matrix into regions with a multilayer periodicity of $\sim \lambda/2$ (Figure 2c).⁵³ Supporting Information Figure S1 shows the recording setup. When the reflected frequency is in phase with the incident beam, where the light intensity is maximum, the standing wave produces dark (node) and bright fringe (antinode) regions.⁵⁴ Using a photographic developer, the

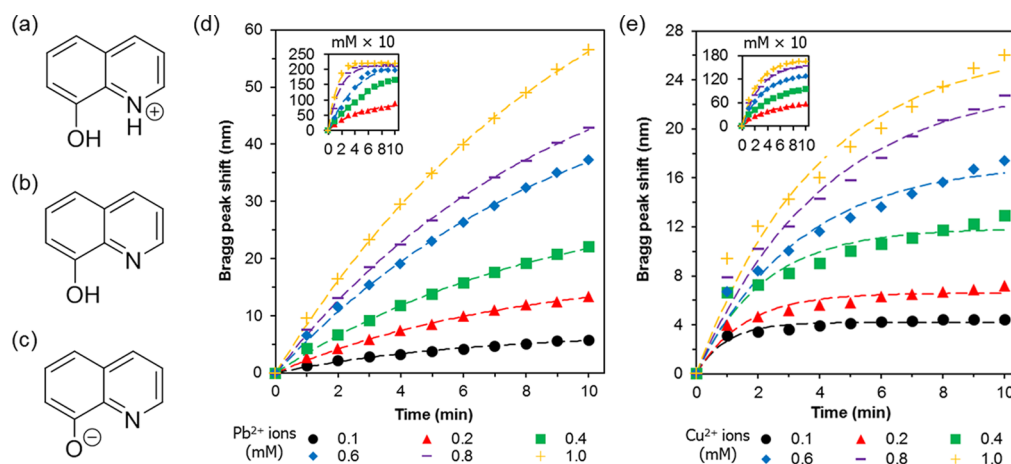


Figure 4. Prototropic forms of 8HQ and sensor reversibility. (a) The protonated quinolinium form ($\text{pH} < 3.0$), (b) the neutral enolic 8HQ form ($\text{pH} = 7.0$), and (c) the deprotonated quinolate form 8HQ ($\text{pH} > 12.0$). (d) Sensor readouts over 10 min in response to variation in the concentrations of Pb^{2+} and (e) Cu^{2+} ions from 0.1 to 1.0 mM in acetate buffers ($\text{pH} 4.2$, 200 mM) at 24 °C. The insets show the readouts from 2.0 to 10.0 mM. The dashed lines represent the fitting according to the exponential decay eq 2. Standard error bars represent three independent trials. The initial Bragg peak (λ_{peak}) is 637.0 ± 0.8 nm.

latent image-comprising AgBr NCs in the antinode regions were reduced to Ag^0 NPs (Figure 2d), hypoed with a $\text{Na}_2\text{S}_2\text{O}_3$ solution (Figure 1e), and bleached with a CuSO_4 and KBr solution (Figure 2f) to obtain periodic AgBr NCs distributed throughout the PAM matrix. The Bragg grating consisted of AgBr NCs ($\phi \sim 5\text{--}20$ nm) periodically organized in multilayer regions within an ~ 10 μm thick PAM matrix. The PAM matrix was functionalized with 5A-8HQ using a DCC-initiated condensation reaction to form an amide linkage, after which the sensor was ready for use (Scheme 1).

RESULTS AND DISCUSSION

Quantification of Pb^{2+} and Cu^{2+} Cation Concentrations. In ambient air (60% RH), the sensor diffracted narrow-band light at 485 nm at $\sim 10^\circ$ from the specular reflection (Figure 3a), and diffraction efficiency was 2 orders of magnitude greater than that at the other wavelengths, confirming the existence of an underlying photonic structure. The diffraction is governed by Bragg's law: $\lambda_{\text{peak}} = 2nd \sin(\theta)$, where λ_{peak} is the wavelength of the first-order diffracted light at the maximum intensity in vacuo, n is the effective index of refraction of the medium, d is the grating spacing, and θ is the Bragg angle, which is determined by the recording geometry. Introduction of an acetate buffer ($\text{pH} 4.20$, 200 mM) at 24 °C to the sensor caused a red Bragg shift from 485 to 637 nm. At $\text{pH} 4.20$, the PAM matrix was partially protonated, and in the presence of the counteranions and water, the matrix expanded and shifted the Bragg peak to longer wavelengths. Upon interaction with a target metal cation, the 8HQ-functionalized sensor actuated a volumetric change, which was reported through blue Bragg shifts. Upon chelation of a divalent metal ion, the formation of bisligand complexes between neutral enolic 8HQ molecules decreased the Donnan osmotic pressure within the PAM matrix, resulting in water expulsion, shrinkage of the matrix, and closer nanocrystal spacing. A decrease in the lattice spacing of AgBr NCs, primarily in the vertical direction underlying its substrate, shifted the Bragg peak to shorter wavelengths. Supporting Information Figure S2 shows the interrogation setup. The amount and the speed of change in the position of the Bragg peak were correlated with the concentration of the target metal cation. Figure 3b shows a

typical sensor response when the divalent metal ion free acetate buffer ($\text{pH} 4.20$) was replaced by an acetate buffer containing Pb^{2+} ions (0.2–2.0 mM), which shifted the Bragg peak from 637 to 550 nm. Inset in Figure 3b illustrates the colorimetric response, which allowed semiquantitative readouts by eye.

The changes in the AgBr NC spacing through the modulation of the diffracted light allowed the quantification of metal cations. Due to the high 2:1 association constant, the bisligand Pb^{2+} ions could not be removed from the PAM matrix by rinsing with a divalent metal ion free acetate buffer solution. In order to reuse the sensor, the PAM matrix was agitated for 3 min with an EDTA solution. EDTA is a hexadentate chelating agent that can bind to metal ions, and it is used in chelation therapy in treating lead and mercury poisoning.⁵⁵ EDTA binds to metal ions by its four carboxylates and two amines to form a compound in octahedral geometry or seven-coordinate complexes. After complexation with EDTA, metal ions exhibit reduced reactivity, and the chelation of metal ions with EDTA reset the diffraction peak to its original position ($\lambda_{\text{peak}} = 637$ nm). All the measurements were conducted using the same sensor with the EDTA solution to reset the Bragg peak position over 100 times. Since the spectrophotometer had a resolution of 0.5 nm wavelength shift, a minimum AgBr NC lattice swelling distance of 0.18 nm produced a resolvable Bragg peak shift corresponding to a total PAM matrix swelling of ~ 9.7 nm (Supporting Information). Figure 3c shows the Bragg shifts of the sensor in response to alkali, alkaline earth, transition, and post-transition metals in acetate buffers ($\text{pH} 4.2$, 200 mM) at 24 °C. While the blue Bragg peak shift for alkali earth metals (1.0 mM) was ~ 3 nm over 10 min, for Pb^{2+} and Cu^{2+} ions at the same molarity, the peak shifted by 57 and 25 nm, respectively. Figure 3d illustrates the blue Bragg shifts in response to increasing concentrations of Pb^{2+} and Cu^{2+} ions from 0.1 to 1.0 mM over 10 min. When the concentrations of Pb^{2+} and Cu^{2+} ions were increased to 10.0 mM, the Bragg peak shifted by 225 and 175 nm over 10 min (inset in Figure 3d).

Dynamic Modulation of the Photonic Nanosensor. The chelation of metal ions with 8HQ is pH-dependent. At $\text{pH} 4\text{--}7$, 8HQ has high affinity for Pb^{2+} and Cu^{2+} ions.^{56,57} Figure 4a–c shows the prototropic forms of 8HQ. The ground-state $\text{p}K_a$ values of 8HQ in aqueous solutions are 5.13 ($\geq \text{NH}^+/\geq \text{N}$)

and 9.89 ($-\text{OH}/-\text{O}^-$).^{58,59} At pH values lower than 3.0, 8HQ is in the protonated quinolinium form (C) (Figure 4a), at a pH value of 7.0, the predominant form is the neutral enolic 8HQ(N) form (Figure 4b), and at pH values higher than 12, it is in the deprotonated quinolate 8HQ(A) form (Figure 4c). Its chelation potential is highest in its neutral enolic 8-HQ(N) form. This cationic selectivity can be explained by the Pearson's hard and soft acid base concept.⁶⁰ Pb^{2+} and Cu^{2+} cations are soft acids, and they have a tendency to bind with soft bases such as pyridine and quinolone. At acidic pH (≈ 4.2) quinolium ion (NH^+), proton (H^+ , a hard acid) can be replaced by soft acids such as $\text{Pb}^{2+}/\text{Cu}^{2+}$ cations. When the concentration of the Pb^{2+} and Cu^{2+} ions increased in the PAM matrix over 10 min, the binding mechanism became kinetically slower due to the reduction of available neutral enolic 8HQ(N) molecules and changes in the elasticity of the PAM matrix. By analyzing the blue Bragg peak shift, the characteristics of the sensor was predicted at a given Pb^{2+} or Cu^{2+} ion concentration. The saturation in bisligand complexation at a given time point t can be expressed as an exponential decay:

$$C_i(t) = C_\infty(1 - e^{-\nu t}) \quad (1)$$

where C_∞ is the amount of enolic 8HQ(N) form at infinite time and ν represents the rate of bisligand complexation. Assuming that the complexation is proportional to the Bragg shift $\Delta\lambda(t)$, this relationship can be expressed as

$$\Delta\lambda(t) = \Delta\lambda_\infty(1 - e^{-\nu t}) \quad (2)$$

where $\Delta\lambda_\infty$ is the equilibrated Bragg shift. Hence, eq 2 can be used to describe the saturation of the Bragg peak in time. Figure 4, parts d and e, shows the blue Bragg peak shifts over 10 min in response to changes in the concentration of Pb^{2+} and Cu^{2+} ions from 0.1 to 1.0 mM in acetate buffers (pH 4.2, 200 mM) at 24 °C, showing limits of detection of 11.4 and 18.6 μM . The insets in Figure 4, parts d and e, show the readouts for changes in the Pb^{2+} and Cu^{2+} ion concentrations from 2.0 to 10.0 mM over 10 min. Equation 2 is an accurate fit for the change in the rate of the bisligand complexation in time (Figure 4, parts d and e). Supporting Information Figure S3 illustrates the Bragg shift as a function of Pb^{2+} and Cu^{2+} ion concentrations as the time approaches infinite according to the fit in Figure 4, parts d and e, and Supporting Information Figure S3b shows the time constant (ν) for different concentrations. Additionally, Supporting Information Figure S4 shows the readouts for alkali, alkaline earth, and transition metals (1.0 mM) over 10 min.

In addition to photonic nanosensor technology, several advances in metal cation sensing have been demonstrated. For example, electrochemical stripping analysis is a sensitive technique that allows detection limits of 8.7 nmol L^{-1} in the working range of 4.8 nmol L^{-1} to 9.6 $\mu\text{mol L}^{-1}$.⁶¹ Similarly, ion-selective electrodes offer detection limits down to 0.63 μM in the working range of 3.2 μM to 31.6 mM.⁶² Recently, DNAzyme- and glutathione-functionalized plasmonic gold nanoparticles achieved detection limits from 1 pM to 100 nM in the range of 1 pM to 10.0 μM .^{63,64} In comparison to these sensitive detection methods, the presented nanosensor offers an alternative to measure Pb^{2+} cations at high concentrations (0.1–10.0 mM). However, the sensitivity may be improved by decreasing the concentration of the MBAM and/or increasing the concentration of carboxylic acid moieties in the PAM matrix.

CONCLUSIONS

We have demonstrated a strategy to fabricate a divalent metal cation sensor via laser writing. We used a single laser pulse (6 ns, 532 nm) to form a slanted diffraction grating, which consisted of periodic AgBr NC regions within an 8HQ-functionalized PAM matrix. By changing the lattice spacing of grating, the sensor was modulated to diffract narrow-band light within the visible region of the spectrum ($\lambda_{\text{peak}} \approx 400\text{--}640$ nm). When used in combination with an EDTA solution, the sensor displayed reversible response to variation in the concentrations (0.1–10.0 mM) of metal cations such as Pb^{2+} and Cu^{2+} . However, hydrogel-based sensors can be functionalized to sense a range of physical parameters and analytes.^{65,66} We envision that NC hydrogel sensors can be multiplexed with microfluidic devices^{67–71} and contact lens sensors,⁷² and readouts can be quantified by smartphone applications.^{73,74}

Our method has compatibility with a diverse array of substrate matrixes from synthetic to natural polymers. The angle of diffraction and its pattern can be controlled by changing the laser exposure conditions, such as humidity, and the geometry (tilt angle) of the object. The Bragg peak of the diffraction grating can be tuned by changing the wavelength of the laser light and choosing a corresponding photosensitizing dye such as 1,1'-diethyl-2,2'-cyanine, 1,1'-diethyl-2,2'-carbocyanine, or *N,N,N',N'*-tetraethylrhodamine. Such well-ordered diffraction gratings can be built from metallic nanoparticles and dyes, and low-cost laser pointers can be used to produce the diffraction gratings in the visible spectrum as well as in near-infrared. Laser writing allows flexible patterning, and enables the production of a low-cost and scalable photonic sensor. We envision that our platform technology for fabricating metal cation sensors with wide optical ranges will lead to applications from printable devices to equipment-free colorimetric sensors.

ASSOCIATED CONTENT

Supporting Information

Interrogation setup, fit constants, readouts for mono/divalent cations, and theoretical background and resolution. This material is available free of charge via the Internet at <http://pubs.acs.org>.

AUTHOR INFORMATION

Corresponding Author

*E-mail: ay283@cam.ac.uk.

Author Contributions

A.K.Y. and M.M.Q. designed the project, carried out the synthesis, and fabricated the sensors. A.K.Y. carried out the measurements. A.K.Y. and Y.M. analyzed the data. H.B. performed the simulations. T.D.W. contributed new reagents. A.K.Y. wrote the manuscript. M.J.M. and Y.M. edited the manuscript.

Notes

The authors declare no competing financial interest.

ACKNOWLEDGMENTS

We thank Christopher R. Lowe for purchasing 8HQ and allowing us to use the laser setup and the spectrophotometer. We also thank Jeff Blyth for the discussions and help in the preliminary experiments. The project was carried out in the Centre of Molecular Materials for Photonics and Electronics at the University of Cambridge.

REFERENCES

- (1) Waldron, K. J.; Rutherford, J. C.; Ford, D.; Robinson, N. J. *Nature* **2009**, *460*, 823–830.
- (2) Jung, J. H.; Lee, J. H.; Shinkai, S. *Chem. Soc. Rev.* **2011**, *40*, 4464–4474.
- (3) Kim, H. N.; Ren, W. X.; Kim, J. S.; Yoon, J. *Chem. Soc. Rev.* **2012**, *41*, 3210–3244.
- (4) Albelda, M. T.; Frias, J. C.; Garcia-Espana, E.; Schneider, H. J. *Chem. Soc. Rev.* **2012**, *41*, 3859–3877.
- (5) Dudev, T.; Lim, C. *Chem. Rev.* **2014**, *114*, 538–556.
- (6) Bings, N. H.; Bogaerts, A.; Broekaert, J. A. *Anal. Chem.* **2010**, *82*, 4653–4681.
- (7) Profrock, D.; Prange, A. *Appl. Spectrosc.* **2012**, *66*, 843–868.
- (8) Liu, R.; Wu, P.; Yang, L.; Hou, X.; Lv, Y. *Mass Spectrom. Rev.* **2014**, *33*, 373–393.
- (9) Lodeiro, C.; Capelo, J. L.; Mejuto, J. C.; Oliveira, E.; Santos, H. M.; Pedras, B.; Nunez, C. *Chem. Soc. Rev.* **2010**, *39*, 2948–2976.
- (10) Zhao, Q.; Li, F.; Huang, C. *Chem. Soc. Rev.* **2010**, *39*, 3007–3030.
- (11) Wegner, S. V.; Okesli, A.; Chen, P.; He, C. *J. Am. Chem. Soc.* **2007**, *129*, 3474–3475.
- (12) Huang, C. C.; Yang, Z.; Lee, K. H.; Chang, H. T. *Angew. Chem., Int. Ed.* **2007**, *46*, 6824–6828.
- (13) Nolan, E. M.; Lippard, S. J. *J. Am. Chem. Soc.* **2007**, *129*, 5910–5918.
- (14) Zhang, X.; Lovejoy, K. S.; Jasanoff, A.; Lippard, S. J. *Proc. Natl. Acad. Sci. U. S. A.* **2007**, *104*, 10780–10785.
- (15) Cheng, T.; Xu, Y.; Zhang, S.; Zhu, W.; Qian, X.; Duan, L. *J. Am. Chem. Soc.* **2008**, *130*, 16160–16161.
- (16) Taki, M.; Desaki, M.; Ojida, A.; Iyoshi, S.; Hirayama, T.; Hamachi, I.; Yamamoto, Y. *J. Am. Chem. Soc.* **2008**, *130*, 12564–12565.
- (17) Zhang, X. A.; Hayes, D.; Smith, S. J.; Friedle, S.; Lippard, S. J. *J. Am. Chem. Soc.* **2008**, *130*, 15788–15789.
- (18) Ye, B. C.; Yin, B. C. *Angew. Chem., Int. Ed.* **2008**, *47*, 8386–8389.
- (19) Tomat, E.; Nolan, E. M.; Jaworski, J.; Lippard, S. J. *J. Am. Chem. Soc.* **2008**, *130*, 15776–15777.
- (20) Chatterjee, A.; Santra, M.; Won, N.; Kim, S.; Kim, J. K.; Kim, S. B.; Ahn, K. H. *J. Am. Chem. Soc.* **2009**, *131*, 2040–2041.
- (21) Marbella, L.; Serli-Mitasev, B.; Basu, P. *Angew. Chem., Int. Ed.* **2009**, *48*, 3996–3998.
- (22) Huang, L.; Hou, F. P.; Xi, P.; Bai, D.; Xu, M.; Li, Z.; Xie, G.; Shi, Y.; Liu, H.; Zeng, Z. *J. Inorg. Biochem.* **2011**, *105*, 800–805.
- (23) Lee, J. S.; Han, M. S.; Mirkin, C. A. *Angew. Chem., Int. Ed.* **2007**, *46*, 4093–4096.
- (24) Wang, Z. D.; Lee, J. H.; Lu, Y. *Adv. Mater.* **2008**, *20*, 3263–3267.
- (25) Li, T.; Dong, S. J.; Wang, E. *Anal. Chem.* **2009**, *81*, 2144–2149.
- (26) Wang, H.; Kim, Y.; Liu, H.; Zhu, Z.; Bamrungsap, S.; Tan, W. J. *Am. Chem. Soc.* **2009**, *131*, 8221–8226.
- (27) Xiang, Y.; Tong, A.; Lu, Y. *J. Am. Chem. Soc.* **2009**, *131*, 15352–15357.
- (28) Yin, B. C.; Ye, B. C.; Tan, W.; Wang, H.; Xie, C. C. *J. Am. Chem. Soc.* **2009**, *131*, 14624–14625.
- (29) Li, T.; Dong, S.; Wang, E. *J. Am. Chem. Soc.* **2010**, *132*, 13156–13157.
- (30) Mor-Piperberg, G.; Tel-Vered, R.; Elbaz, J.; Willner, I. *J. Am. Chem. Soc.* **2010**, *132*, 6878–6879.
- (31) Dave, N.; Chan, M. Y.; Huang, P. J. J.; Smith, B. D.; Liu, J. W. *J. Am. Chem. Soc.* **2010**, *132*, 12668–12673.
- (32) Lee, S. J.; Lee, J. E.; Seo, J.; Jeong, I. Y.; Lee, S. S.; Jung, J. H. *Adv. Funct. Mater.* **2007**, *17*, 3441–3446.
- (33) Wu, C.-S.; Oo, M. K. K.; Fan, X. *ACS Nano* **2010**, *4*, 5897–5904.
- (34) Lee, J.; Jun, H.; Kim, J. *Adv. Mater.* **2009**, *21*, 3674–3677.
- (35) Kagan, D.; Calvo-Marzal, P.; Balasubramanian, S.; Sattayasamitsathit, S.; Manesh, K. M.; Flechsig, G.-U.; Wang, J. *J. Am. Chem. Soc.* **2009**, *131*, 12082–12083.
- (36) Zhou, Y.; Wang, S.; Zhang, K.; Jiang, X. *Angew. Chem., Int. Ed.* **2008**, *47*, 7454–7456.
- (37) Zhang, T.; Cheng, Z.; Wang, Y.; Li, Z.; Wang, C.; Li, Y.; Fang, Y. *Nano Lett.* **2010**, *10*, 4738–4741.
- (38) Sudibya, H. G.; He, Q.; Zhang, H.; Chen, P. *ACS Nano* **2011**, *5*, 1990–1994.
- (39) Liu, Y.; Dong, X.; Chen, P. *Chem. Soc. Rev.* **2012**, *41*, 2283–2307.
- (40) Yetisen, A. K. *Holographic Sensors*; Springer International Publishing Switzerland: Cham, Switzerland, 2015; pp 85–99.
- (41) Yetisen, A. K.; Montelongo, Y.; da Cruz Vasconcellos, F.; Martinez-Hurtado, J. L.; Neupane, S.; Butt, H.; Qasim, M. M.; Blyth, J.; Burling, K.; Carmody, J. B.; Evans, M.; Wilkinson, T. D.; Kubota, L. T.; Monteiro, M. J.; Lowe, C. R. *Nano Lett.* **2014**, *14*, 3587–3593.
- (42) Yetisen, A. K.; Butt, H.; da Cruz Vasconcellos, F.; Montelongo, Y.; Davidson, C. A. B.; Blyth, J.; Chan, L.; Carmody, J. B.; Vignolini, S.; Steiner, U.; Baumberg, J. J.; Wilkinson, T. D.; Lowe, C. R. *Adv. Opt. Mater.* **2014**, *2*, 250–254.
- (43) Yetisen, A. K.; Qasim, M. M.; Nosheen, S.; Wilkinson, T. D.; Lowe, C. R. *J. Mater. Chem. C* **2014**, *2*, 3569.
- (44) Tsangarides, C. P.; Yetisen, A. K.; Vasconcellos, F. D.; Montelongo, Y.; Qasim, M. M.; Wilkinson, T. D.; Lowe, C. R.; Butt, H. *RSC Adv.* **2014**, *4*, 10454–10461.
- (45) Aragay, G.; Pons, J.; Merkoci, A. *Chem. Rev.* **2011**, *111*, 3433–3458.
- (46) Ma, R. M.; Ota, S.; Li, Y.; Yang, S.; Zhang, X. *Nat. Nanotechnol.* **2014**, *9*, 600–604.
- (47) Im, H.; Shao, H.; Park, Y. I.; Peterson, V. M.; Castro, C. M.; Weissleder, R.; Lee, H. *Nat. Biotechnol.* **2014**, *32*, 490–495.
- (48) Oh, J. W.; Chung, W. J.; Heo, K.; Jin, H. E.; Lee, B. Y.; Wang, E.; Zueger, C.; Wong, W.; Meyer, J.; Kim, C.; Lee, S. Y.; Kim, W. G.; Zemla, M.; Auer, M.; Hexemer, A.; Lee, S. W. *Nat. Commun.* **2014**, *5*, 3043.
- (49) Paek, K.; Yang, H.; Lee, J.; Park, J.; Kim, B. J. *ACS Nano* **2014**, *8*, 2848–2856.
- (50) Stein, A.; Wilson, B. E.; Rudisill, S. G. *Chem. Soc. Rev.* **2013**, *42*, 2763–2803.
- (51) Fenzl, C.; Hirsch, T.; Wolfbeis, O. S. *Angew. Chem., Int. Ed.* **2014**, *53*, 3318–3335.
- (52) Blyth, J.; Millington, R. B.; Mayes, A. G.; Lowe, C. R. *Imaging Sci. J.* **1999**, *47*, 87–91.
- (53) Yetisen, A. K.; Montelongo, Y.; Farandos, N. M.; Naydenova, I.; Lowe, C. R.; Yun, S. H. *Appl. Phys. Lett.* **2014**, *105*, 261106.
- (54) Vasconcellos, F. d. C.; Yetisen, A. K.; Montelongo, Y.; Butt, H.; Grigore, A.; Davidson, C. A. B.; Blyth, J.; Monteiro, M. J.; Wilkinson, T. D.; Lowe, C. R. *ACS Photonics* **2014**, *1*, 489–495.
- (55) Andersen, O. *Chem. Rev.* **1999**, *99*, 2683–2710.
- (56) Allen, E. A.; Bartlett, P. K. N.; Ingram, G. *Analyst* **1984**, *109*, 1075–1080.
- (57) Martins, A. O.; da Silva, E. L.; Laranjeira, M. C. M.; de Favere, V. T. *Microchim. Acta* **2005**, *150*, 27–33.
- (58) Albert, A.; Phillips, J. N. *J. Chem. Soc.* **1956**, 1294.
- (59) Bardez, E.; Devol, I.; Larrey, B.; Valeur, B. *J. Phys. Chem. B* **1997**, *101*, 7786–7793.
- (60) Pearson, R. G. *J. Am. Chem. Soc.* **1963**, *85*, 3533–3539.
- (61) Guell, R.; Aragay, G.; Fontas, C.; Antico, E.; Merkoci, A. *Anal. Chim. Acta* **2008**, *627*, 219–224.
- (62) Huang, M. R.; Rao, X. W.; Li, X. G.; Ding, Y. B. *Talanta* **2011**, *85*, 1575–1584.
- (63) Chai, F.; Wang, C. A.; Wang, T. T.; Li, L.; Su, Z. M. *ACS Appl. Mater. Interfaces* **2010**, *2*, 1466–1470.
- (64) Pelossof, G.; Tel-Vered, R.; Willner, I. *Anal. Chem.* **2012**, *84*, 3703–3709.
- (65) Yetisen, A. K.; Naydenova, I.; da Cruz Vasconcellos, F.; Blyth, J.; Lowe, C. R. *Chem. Rev.* **2014**, *114*, 10654–10696.
- (66) Naydenova, I.; Jallapuram, R.; Toal, V.; Martin, S. *Appl. Phys. Lett.* **2008**, *92*, 031109.
- (67) Yetisen, A. K.; Akram, M. S.; Lowe, C. R. *Lab Chip* **2013**, *13*, 2210–2251.

(68) Volpatti, L. R.; Yetisen, A. K. *Trends Biotechnol.* **2014**, *32*, 347–350.

(69) Yetisen, A. K.; Volpatti, L. R. *Lab Chip* **2014**, *14*, 2217–2225.

(70) Akram, M.; Daly, R.; da Cruz Vasconcellos, F.; Yetisen, A.; Hutchings, I.; Hall, E. H. In *Lab-on-a-Chip Devices and Micro-Total Analysis Systems*; Castillo-León, J., Svendsen, W. E., Eds.; Springer International Publishing Switzerland: Cham, Switzerland, 2015; pp 161–195.

(71) Yetisen, A. K.; Jiang, L.; Cooper, J. R.; Qin, Y.; Palanivelu, R.; Zohar, Y. *J. Micromech. Microeng.* **2011**, *21*, 054018.

(72) Farandos, N. M.; Yetisen, A. K.; Monteiro, M. J.; Lowe, C. R.; Yun, S. H. *Adv. Healthcare Mater.* **2014**, DOI: 10.1002/adhm.201400504.

(73) Yetisen, A. K.; Martinez-Hurtado, J. L.; da Cruz Vasconcellos, F.; Simsekler, M. C.; Akram, M. S.; Lowe, C. R. *Lab Chip* **2014**, *14*, 833–840.

(74) Yetisen, A. K.; Martinez-Hurtado, J. L.; Garcia-Melendrez, A.; Vasconcellos, F. D.; Lowe, C. R. *Sens. Actuators, B* **2014**, *196*, 156–160.